Int J Adv Manuf Technol (2017) 93:2985–2996
DOI 10.1007/s00170-017-0653-y

ORIGINAL ARTICLE

Three-dimensional numerical simulation for drilling of 2.5D carbon/carbon composites

Chenwei Shan[1] · **Jie Dang**[1] · **Jiaqiang Yan**[1] · **Xu Zhang**[1]

Received: 4 January 2017 / Accepted: 5 June 2017 / Published online: 12 July 2017

Abstract Drilling of carbon/carbon (C/C) composites is difficult to implement due to the materials' high specific stiffness, brittleness, anisotropic, heterogeneous, and low thermal conductivity, resulting in tear, burr, poor surface quality, and rapid wear of cutters. Accurate and fast predictions of thrust forces and defects are important for C/C composites drilling process with high quality. In this paper, a finite element analysis method for drilling of 2.5D C/C composites is presented. An improved damage initiation model is proposed based on the Shokrieh-Lessard's model and the Hashin's failure criteria. Six different failure modes—X-direction fiber-matrix tension, X-direction fiber-matrix compression, Y-direction tension, Y-direction compression, normal tension, and normal compression—are considered and modeled separately. An improved 3D progressive failure model is developed to approximate real failure process of 2.5D C/C composites. For validation purpose, drilling tests have been performed and compared to the results of finite element analysis. The experimental result shows to be consistent well with the proposed model, yielding a relative difference of predicted thrust force from 8.07 to 13.86%. The model demonstrates its ability to predict thrust force, material failure process, and damage for different values of feedrate.

Keywords C/C composites · Thrust force · Drilling · Finite element analysis · Progressive failure model

✉ Chenwei Shan
shancw@nwpu.edu.cn

[1] Key Laboratory of Contemporary Design and Integrated Manufacturing Technology, Ministry of Education, Northwestern Polytechnical University, Xi'an 710072, China

1 Introduction

C/C composites are carbon-fiber-reinforced carbon matrix composites. They offer some superior properties, such as high heat resistance, along with lightweight, low thermal expansion coefficient, and high resistance to corrosion [1, 2]. C/C composites retain room temperature properties to be more than 3000 °C in the inert atmosphere, and this is the main trend of the development of ultra-high-temperature structural materials in the future [3]. In addition, C/C composites are capable of replacing heart valves and hip due to its excellent biological compatibility [4].

There are several kinds of C/C composites according to their braided structures. One is called 2.5-dimensional (2.5D) C/C composite. The microstructure of the 2.5D C/C composite with needle-punched felt is shown in Fig. 1 [5]. Although reinforced by needle-punched felt, this material is strong in the fiber direction, but quite weak in the needle-punched direction. This makes it easily crush.

Conventional machining operations of C/C composites, such as turning, milling, and drilling, which are a problem as the fibers and fiber direction result in an uneven cutting force and high tool wear, can still be applied to the machining of C/C composites. The electro-discharge machining (EDM) method also can be used to machine C/C composites [6, 7]. Drilling operations are often required before mechanical joining of the C/C composites components. Conventional twist drilling is a fast, effective, and commonly used hole-making method for secondary machining of composite structures. Due to the economic reasons, the two-flute conventional twist drill (used for the drilling of metallic materials) is adopted to drill composite structures [8]. However, some characteristics of C/C composites such as nonhomogeneity, anisotropy, highly abrasive and hard reinforced carbon fibers, high specific stiffness, brittleness, and low thermal conductivity make it

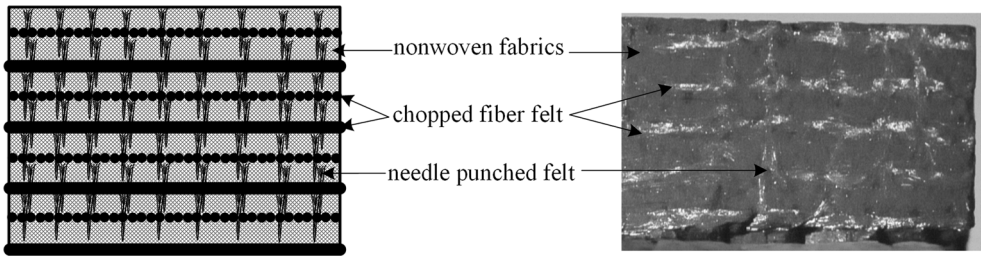

Fig. 1 Illustration of 2.5D C/C composite structure [5]

difficult to machine. The most frequent drilling-induced defects are tear, burr, delamination, edge breakage in addition to other minor damages. Since stress concentrates at holes under loading and the surface quality plays an important role in the improvement of fatigue life of composite, it is necessary to decrease the defects in drilling of C/C composites [9].

Although nearly 60 years have passed since C/C composites appeared for the first time, there is little work about milling, turning, and drilling of C/C composites. Ferreira et al. [10] researched the turning process of C/C composites by experimental methods. The experimental results illustrated that polycrystalline diamond (PCD) was the optimal tool in finish turning, and cemented carbide tools could be used in rough turning with appropriate cutting parameters.

Compared with conventional milling, Li et al. [11] found that the ultrasonic-assisted milling could improve the surface quality of C/C composites with lower cutting force, tool wear, and cutting temperature. It is helpful to process C/C composites with high efficiency, high precision, and low cost. Shan et al. [12] analyzed the defects caused in conventional twist drilling of 2.5D C/C composites, and the fiber fuzz factor and the ripping factor are defined to depict the drilling defects. Subsequently, Shan et al. [5] presented an alternative cutting force model involving the influences of the directions of fiber. Based on the calculated and experimental results, the cutting forces' coefficients of 2.5D C/C composites are evaluated using multiple linear regression method.

Although little work has been done on drilling of C/C composites, there are many researches focusing on drilling of fiber-reinforced polymer composite (FRP). Polymeric composites are recognized as good candidates for structural components due to their inherent properties [13]. Abrao et al. [14] investigated the effect of the cutting tool geometry and material on the thrust force and delamination produced when drilling a glass fiber-reinforced epoxy composite using drills with different geometry and material. Rubio et al. [15] found that high speed machining is a reasonable drilling method for glass fiber-reinforced polymer composite (GFRP) which reduces damage by experiments. Davim et al. [16] presented a method to measure the delamination factor using digital analysis, which is suitable to estimate the damages produced after drilling CFRP. Gaitonde et al. [17] found that the delamination tendency decreases with increase in cutting speed in high speed drilling of CFRP by experiments, and the low values of feed rate and point angle combination are useful for reducing the damage. Singh et al. [18] studied how drilling parameters influence drilling-induced damage by using the digital image processing technique. The results showed tool point geometry is a major factor that influences drilling-induced damage.

Simulation of drilling process is an effective method that can be used to optimize drill geometry and process parameters in order to control hole quality and analyze the drill wear evolution [19]. Compared with analytical methods, finite element analysis (FEA) holds plenty of advantages; by FEA, one can obtain not only the global variable like thrust force and the shape of chip, but also one can obtain the specific stress and temperature distribution at an interested point [20]. Many finite element (FE) model studies have been conducted to predict cutting forces and delamination of composites. FEA allows controlling all variables that take part during the machining process and uncoupling the influencing parameters. Excellent reviews on composite machining can be found in [21–23].

There are a few works focusing on numerical modeling of composite drilling. Most literatures presenting numerical modeling of CFRP cutting focus on orthogonal cutting due to its simplicity. FEA of orthogonal cutting of fiber-reinforced composite was proposed by Arula and Ramulu using maximum stress and Tsai-Hill criteria [24]. Some examples of the modeling strategies and material modeling used in scientific literature for two-dimensional (2D) approach to simulation of orthogonal cutting of CFRPs can be found in [25–27].

Drilling of composite materials has been simulated as three-dimensional (3D) orthogonal cutting using FEA. Recently, numerical predictions of critical thrust force and delamination have been performed in drilling of CFRPs [28–30].

Based on the fracture mechanics, Zitoune and Collombet [28] proposed a numerical FEA model of drilling of unidirectional CFRPs to predict cutting force and delamination by simplification to orthogonal model. The validation of this model was carried out on two types of carbon/epoxy long fiber materials. However, its validity was not been fully proved on laminated from weaved sheet. In order to simulate thrust forces and delamination onset during drilling carbon/epoxy composites, Durao et al. [29] developed a FE model considering solid elements of the Abaqus software library and

interface elements including a cohesive damage model. Although the numerical and experimental thrust force curves agreed well, the FE model simulation cannot remove plate material continuously. Based on Lagrangian formulation, Isbilir and Ghassemieh [30] developed a 3D FE model to simulate the effects of cutting speed and feedrate on thrust force, torque, and delamination in the drilling of unidirectional CFRPs. Subsequently, based on the Hashin's theory [31], Isbilir and Ghassemieh [32] developed another 3D FE model for drilling CFRPs. In this model, a 3D progressive intra-laminar delamination model and a progressive inter-laminar delamination model are considered and developed. This model could be used as a design tool for drill geometry for minimization of delamination in CFRP drilling. Phadnis et al. [33] developed a 3D FE model of drilling CFRPs, accounting for complex kinematics at the drill-workpiece interface. Both Hashin's and Puck's criteria [31, 34] were implemented in a user-defined material model (VUMAT) in the general-purpose FE software Abaqus/Explicit. The FE model predicted the drilling thrust force and torque with reasonable accuracy when compared to experimental results. Feito et al. [19] presented a FE model for drilling woven CFRPs. Two different point angles considering fresh and honed edge were modeled. This model was able to predict thrust force and delamination for different values of feedrate and cutting speed for drilling CFRPs. The maximum relative difference between the experimental value and the predicted value by regression equations was 13.8% for the thrust force and 2.92% for the delamination.

In this paper, to investigate the effects of cutting speed and feedrate on thrust force and induced damage in the drilling of 2.5D C/C composites, a 3D FEA method is proposed to simulate the 2.5D C/C composites drilling process. To better understand and predict the complex failure mechanisms in drilling of 2.5D C/C composites, an improved damage initiation model and an improved progressive failure analysis model are considered and developed based on the failure models of CFRPs. For validation purposes, experimental drilling tests have been performed and compared to the results of the FEA.

2 Material failure modeling

2.1 Damage initiation

Carbon-fiber-reinforced composite materials including C/C composites display a wide variety of failure mechanisms as a result of their complex structure and manufacturing processes, which include fiber failure, matrix cracking, buckling, and delamination [35].

In this paper, a user-defined 3D damage model (VUMAT) with solid elements is developed and implemented into the FE code Abaqus/Explicit to predict the characteristics and extent of damage through the specimen thickness. The flowchart is shown in Fig. 2.

Orthotropic material properties are assigned to 2.5D C/C composite according to the fiber orientation by using a pre-defined local coordinate system. As shown in Fig. 3, (1) denotes the X-direction along one of the fiber orientation, (2) denotes the Y-direction orthogonal to X-direction, and (3) denotes the Z-direction normal to the fiber layer plane.

Considering there are no any damage initiation criteria being developed for C/C composites, the damage initiation criteria for 2.5D C/C composites in 3D case are developed based on the Shokrieh and Lessard's progressive fatigue damage model [36] in this paper. The Shokrieh and Lessard's progressive fatigue damage model were proposed based on the Hashin's theory [31] to simulate the behavior of composite laminates under general loading conditions. This model is able to predict the residual strength, residual life, final failure mechanisms, and final fatigue life of the composite laminates under general fatigue loading conditions.

The fiber directions of the 2.5D C/C composites are in two orientations, which are different from unidirectional CFRP. The initiation criteria considers six different damage initiation mechanisms, namely X-direction fiber-matrix tension, X-direction fiber-matrix compression, Y-direction tension, Y-direction compression, normal tension, and normal compression as expressed by Eqs. (1)–(6). The compression failure behavior of C/C composites is similar to brittle materials. Shear stress is a main factor that caused the compression failure of brittle materials according to the Mohr strength criterion. Hence,

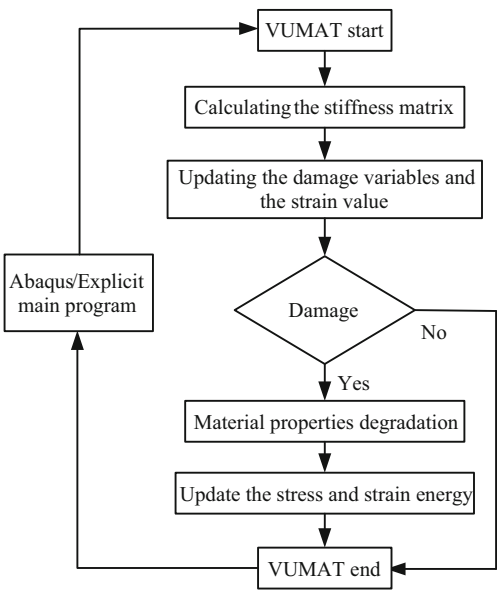

Fig. 2 Flowchart of VUMAT in Abaqus/explicit

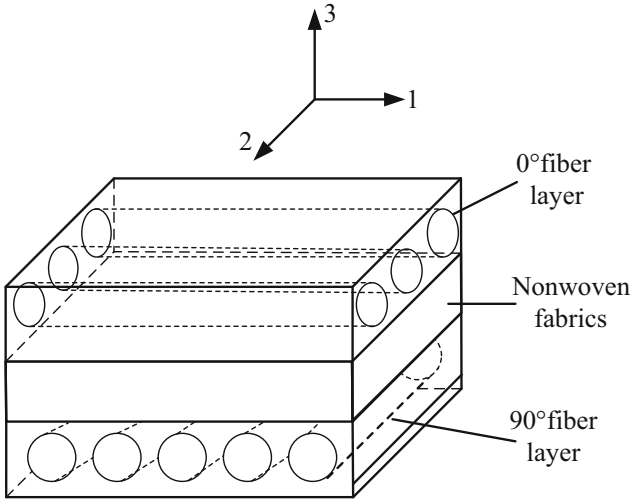

Fig. 3 Definition of local coordinate system: *1* X-direction along one of the fiber orientation, *2* Y-direction, and *3* Z-direction normal to the fiber layer plane

Shear stresses are considered in the tension and compressive directions.

X-direction:

If $\overline{\sigma}_{11} > 0$

$$e_x^t = \left(\frac{\overline{\sigma}_{11}}{X_t}\right)^2 + \alpha\left(\frac{\overline{\tau}_{12}}{S_{12}}\right)^2 + \beta\left(\frac{\overline{\tau}_{13}}{S_{13}}\right)^2 \geq 1 \quad (1)$$

If $\overline{\sigma}_{11} < 0$

$$e_x^c = \left(\frac{\overline{\sigma}_{11}}{X_c}\right)^2 + \left(\frac{\overline{\tau}_{12}}{S_{12}}\right)^2 + \left(\frac{\overline{\tau}_{13}}{S_{13}}\right)^2 \geq 1 \quad (2)$$

Y-direction:

If $\overline{\sigma}_{22} > 0$

$$e_y^t = \left(\frac{\overline{\sigma}_{22}}{Y_t}\right)^2 + \alpha\left(\frac{\overline{\tau}_{12}}{S_{12}}\right)^2 + \beta\left(\frac{\overline{\tau}_{23}}{S_{23}}\right)^2 \geq 1 \quad (3)$$

If $\overline{\sigma}_{22} < 0$

$$e_y^t = \left(\frac{\overline{\sigma}_{22}}{Y_c}\right)^2 + \left(\frac{\overline{\tau}_{12}}{S_{12}}\right)^2 + \left(\frac{\overline{\tau}_{23}}{S_{23}}\right)^2 \geq 1 \quad (4)$$

Normal direction:

If $\overline{\sigma}_{33} > 0$

$$e_z^t = \left(\frac{\overline{\sigma}_{33}}{Z_t}\right)^2 + \left(\frac{\overline{\tau}_{13}}{S_{13}}\right)^2 + \left(\frac{\overline{\tau}_{23}}{S_{23}}\right)^2 \geq 1 \quad (5)$$

If $\overline{\sigma}_{33} < 0$

$$e_z^c = \left(\frac{\overline{\sigma}_{33}}{Z_c}\right)^2 + \left(\frac{\overline{\tau}_{13}}{S_{13}}\right)^2 + \left(\frac{\overline{\tau}_{23}}{S_{23}}\right)^2 \geq 1 \quad (6)$$

where *x, y,* and *z* subscripts denote three directions and *c* and *t* represent compression and tension. $\overline{\sigma}_{11}$, $\overline{\sigma}_{22}$, $\overline{\sigma}_{33}$, $\overline{\tau}_{12}$,$\overline{\tau}_{23}$, and $\overline{\tau}_{13}$ are the effective normal and shear stresses respectively. S_{12}, S_{23} and S_{13} are the in-plane (in the X–Y plane, Y–Z plane, X–Z plane) shear strength. X_t and X_c are the X-direction tensile and compressive strengths. Y_t and Y_c are the Y-direction tensile and compressive strengths. Z_t and Z_c are the normal tensile and compressive strengths.e_x^t, e_x^c, e_y^t, e_y^c, e_z^t, and e_z^c are the failure factors. α and β are the weight coefficients of shear stresses on the X- and Y- directions fiber and matrix tensile failure. The coefficients α and β are set to 1.0 in this paper.

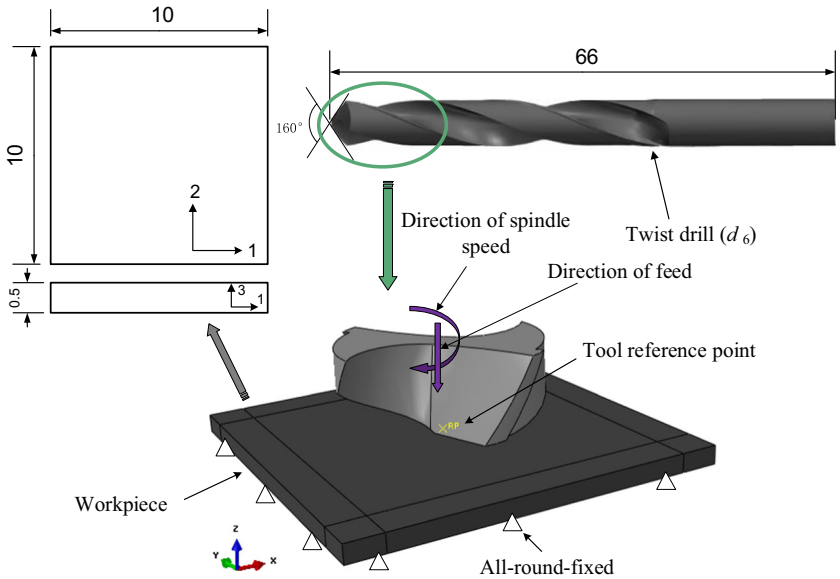

Fig. 4 FE model of drilling 2.5D C/C composite

Table 1 Mechanical properties of 2.5D C/C composite

Properties	Value
ρ(g/cm^3)	1.73
$E_1 = E_2$(Gpa)	31.38
E_3(Gpa)	15.02
G_{12}(Gpa)	8.26
$G_{13} = G_{23}$(Gpa)	3.96
υ_{12}	0.12
$X_t = Y_t$(Mpa)	52.93
$X_c = Y_c$(Mpa)	132.37
Z_t(Mpa)	20.98
Z_c(Mpa)	182.51
S_{12}(Mpa)	91.53
$S_{13} = S_{23}$(Mpa)	21.95

2.2 Progressive failure model

Many fiber-reinforced composite materials exhibit elastic-brittle behavior, that is, damage in these materials, such as C/C composites, is initiated without significant plastic deformation. Consequently, plasticity can be neglected when modeling the behavior of such materials.

According to the Continuum Damage Mechanics (CDM) model originally developed by Kachanov [37], the relation between the effective stress tensor, $\overline{\boldsymbol{\sigma}}$, and the nominal stress tensor, $\boldsymbol{\sigma}$, is postulated to have the form

$$\overline{\boldsymbol{\sigma}} = \mathbf{M}\boldsymbol{\sigma} \tag{7}$$

where $\mathbf{M}$ is a damage effect tensor, which has the diagonal form:

$$\mathbf{M} = \begin{bmatrix} \frac{1}{1-d_1} & 0 & 0 & 0 & 0 & 0 \\ & \frac{1}{1-d_2} & 0 & 0 & 0 & 0 \\ & & \frac{1}{1-d_3} & 0 & 0 & 0 \\ & & & \frac{1}{\sqrt{(1-d_1)(1-d_2)}} & 0 & 0 \\ & & & & \frac{1}{\sqrt{(1-d_1)(1-d_3)}} & 0 \\ sym & & & & & \frac{1}{\sqrt{(1-d_2)(1-d_3)}} \end{bmatrix} \tag{8}$$

where d_1, d_2, and d_3 are damage variables for X-, Y-, and Z-directions failure modes, respectively. The damage tensor $\mathbf{D}$ has the diagonal form:

$$\mathbf{D} = \begin{bmatrix} d_1 & 0 & 0 \\ 0 & d_2 & 0 \\ 0 & 0 & d_3 \end{bmatrix} \tag{9}$$

According to [38], linear behavior, until damage initiation, is generally assumed unless otherwise specified. Once a failure criterion has been met, the material properties are gradually degraded following a nonlinear strain-softening law. The stress-strain constitutive model of the damaged material can be computed by Eq. (10)

$$\boldsymbol{\sigma} = \mathbf{C}_d\boldsymbol{\varepsilon} \tag{10}$$

where $\mathbf{C}_d$ is the damage stiffness matrix, $\boldsymbol{\varepsilon}$ is the nominal strain tensor.

$$\mathbf{C}_d = \mathbf{M}^{-1}\mathbf{C}\mathbf{M}^{T,-1} \tag{11}$$

$$\begin{cases} C_{11}^d = C_{11}\left(1-d' d_1\right)^2 \\ C_{22}^d = C_{22}\left(1-d' d_2\right)^2 \\ C_{33}^d = C_{33}\left(1-d' d_3\right)^2 \\ C_{44}^d = C_{44}\left(1-d' d_1\right)\left(1-d' d_2\right) \\ C_{55}^d = C_{55}\left(1-d' d_1\right)\left(1-d' d_3\right) \\ C_{66}^d = C_{66}\left(1-d' d_2\right)\left(1-d' d_3\right) \\ C_{12}^d = C_{12}\left(1-d' d_1\right)\left(1-d' d_2\right) \\ C_{13}^d = C_{13}\left(1-d' d_1\right)\left(1-d' d_3\right) \\ C_{23}^d = C_{23}\left(1-d' d_2\right)\left(1-d' d_3\right) \end{cases} \tag{12}$$

where $\mathbf{C}$ is the undamaged stiffness matrix of orthotropic materials. Once a damage initiation criterion is satisfied, further loading will cause degradation of material stiffness coefficients. The reduction of the material's stiffness coefficients is controlled by damage variables that might assume values between zero (undamaged state) and one (fully damage state for the mode corresponding to this damage variable) [39]. d' is a coefficient of damage variables, and d' is set to 0.999 to avoid the excessive element distortion in the FEA process.

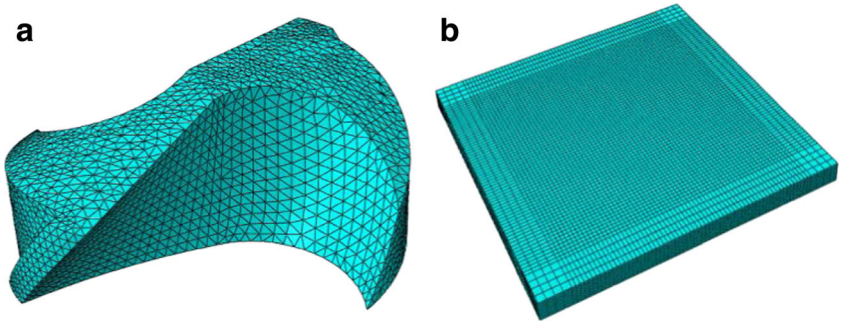

Fig. 5 FE meshes of drill and workpiece. **a** Drill; **b** workpiece

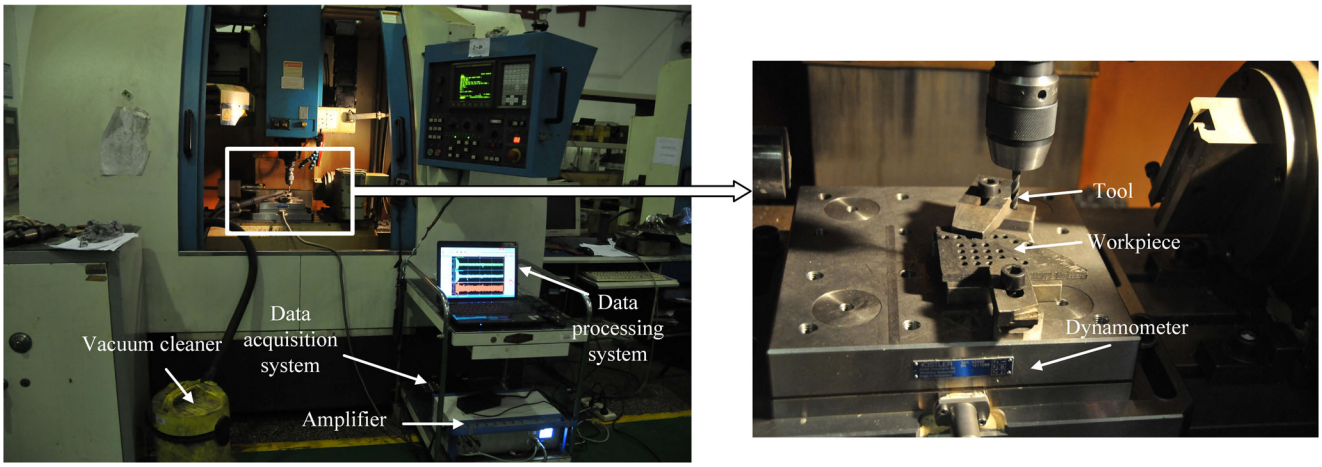

Fig. 6 Experimental setup for drilling 2.5D C/C composite plate

The bi-linear constitutive relationship in Eq. (10) leads to the following damage evolution law.

$$d_i^k(T) = \max_T \left\{ 0, \min \left[1, \frac{\varepsilon_i^{k,f}\left(\varepsilon_i^k - \varepsilon_i^{k,0}\right)}{\varepsilon_i^k\left(\overline{T}\right)\left(\varepsilon_i^{k,f} - \varepsilon_i^{k,0}\right)} \right] \right\}, \forall \overline{T} \le T \tag{13}$$

where T represents the fictitious time that distinguishes each load increment during the FEA and is introduced to account for the irreversibility of the damage, $i = 1, 2, 3$ and $k = t, c$. Where $\varepsilon_i^{k,0} \le \varepsilon_i^k\left(\overline{T}\right) \le \varepsilon_i^{k,f}$. $\varepsilon_i^{k,0}$ is the strain at the onset of failure which depends on the fracture criterion employed, and $\varepsilon_i^{k,f}$ is the strain at failure defined such that the energy dissipated to create the fracture surface is correctly accounted for. $\varepsilon_i^{k,0} = R_i/E_i$, where R_i is the damaged material strength and E_i is the elastic modulus of the damaged material.$\varepsilon_i^{k,f}$ is set to 0.06 according to the reference [40].

Falzon and Apruzzese [41] found that strain localization is a major problem in the FE modeling of material instability phenomena, such as that induced by damage accumulation. As in [41], in the formulation presented, the energy absorbed per unit of cracked area is independent of the mesh refinement and hence the mesh dependency typical of many failure models should be avoided.

Table 2 Machining parameters used in drilling of 2.5D C/C composites

Point angle 2φ	Spindle speed n (rpm)	feedrate v_f (mmpm)
160°	3000	120
		150
		180

According to [38], to correct this behavior, the crack band model proposed by Bažant and Oh [42] can be used. The area under the uniaxial stress–strain curve is adjusted by expressing the strain at failure, ε^f, as a function of the energy release rate, G^f, which is a measure of energy dissipated per unit area, with the energy dissipated per unit volume, the material strength, R, and a characteristic length of the finite element, L_f,

$$\varepsilon^f = \frac{2G^f}{RL_f} \tag{14}$$

L_f is set to 0.05 mm in this paper.

3 Finite element model of drilling

The model presented in this work is able to reproduce drilling of 2.5D C/C composite including chip removal. The FE code Abaqus/Explicit is used to perform the numerical simulations. The complete movement of the drill including feedrate and spindle speed is simulated.

A 3D FE model of drilling is developed which consists of a two-flute conventional carbide twist drill. The drill is modeled in Siemens NX7.5 and imported into the FE software. The 2.5D C/C composite plate and the boundary conditions are shown in Fig. 4. Three degrees of freedom are constrained all round the plate to simulate the fully clamped status. Similarly, the drill is constrained in X- and Y-directions to model the drilling process parameters. The heat generation and tool wear are ignored in the simulation.

A 0.5-mm-thick 2.5D C/C composite plate is used in the model. A local coordinate system is defined to account for orientations of fibers of the plate and material behavior precisely. The material properties of 2.5D C/C composite used in the FEA are shown in Table 1.

Table 3 Experiment and FEA data of thrust force under different drilling condition

No.	Point angle (°)	Spindle speed (rpm)	Feedrate (mmpm)	Thrust force (N)		
				Experiment	FEA	Relative error (%)
1	160°	3000	120	38.79	41.92	8.07
2	160°	3000	150	46.16	52.56	13.86
3	160°	3000	180	52.01	56.83	9.27

Elastic stiffness of the carbide twist drill is in the range of 500–700 GPa as compared to 31.38 GPa for the 2.5D C/C composite in the fiber directions. Hence, in the FEA, the twist drill is modeled as a discrete rigid body with nominal diameter equal to 6 mm to reduce the computational cost involved in the highly resource-consuming drilling simulations.

The twist drill is fed into the workpiece in the axial direction using a velocity boundary condition, which represents the feedrate during experiments. An angular velocity about the drill axis equivalent to the spindle speed of 3000 rpm is superimposed on the drill geometry. Three sets of simulations are carried out with three different feedrates (120,150, and 180 mmpm).

The surface of drill is represented by three node triangular rigid surface elements (R3D3). The drill mesh size is 0.2 mm. In the square C/C composite plate modeled, the plate is represented by eight node brick elements (C3D8R) to reduce computational time and cost. The mesh sensitivity is very important in simulations. Thus, a rigorous mesh sensitivity study is carried out to obtain a computationally accurate finite element mesh. A cuboid mesh size 0.1 mm × 0.1 mm × 0.05 mm in the vicinity of the drilling area is used, while a coarser mesh of 0.25 mm × 0.25 mm × 0.125 mm is used in the area away from the zone of interest. The FE meshes are shown in Fig. 5. Once the failure criteria are satisfied, the failed elements are removed from the FE model.

Contacts between the twist drill and the 2.5D C/C composite plate are defined based on the general contact algorithm available in Abaqus/Explicit. This algorithm generates the contact forces based on the penalty-enforced contact method. The interaction between surfaces (tool/workpiece) is controlled by the Coulomb friction law. The friction coefficient μ is used to account for the shear stress of the surface tractions with the contact pressure p and can be represented as $T = \mu p$. In this case, the frictional contact between a drill and the C/C composite plate is modeled with a constant coefficient of friction of 0.3 used in the drilling of CFRP in the reference [43].

4 Experimental procedure

The drilling experiments are conducted on a JOHNFORD 3-axis vertical machining center with a FANUC-OI-MB NC unit and a maximum speed of 8000 rpm. Two-flute conventional carbide twist drills with diameter 6 mm and a 160° point angle are used. The experimental setup is shown in Fig. 6. A vacuum cleaner is used to collect the cutting chips, as the dry cutting method is used with no coolant.

The experiments are conducted at 3000 rpm at three different feedrates given in Table 2. The thrust force signals during drilling are measured using the Kistler dynamometer 9255B. Dynamometer is charged, and the signals are collected by a data acquisition system which includes a Kistler multi-channel charge amplifier 5019B and Kistler Dynoware software. Experiments are repeated three times, and the results reported are all mean values.

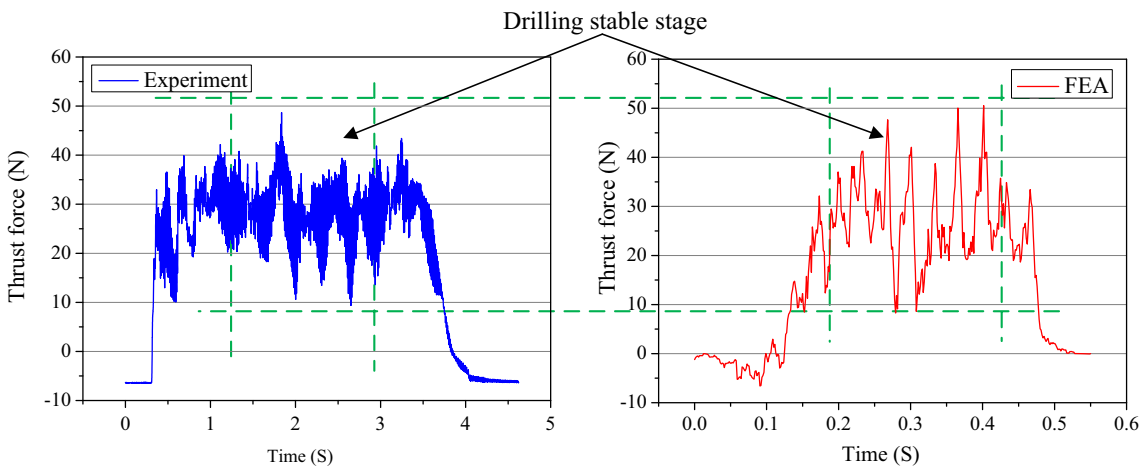

Fig. 7 Experimental and simulation thrust force evolution

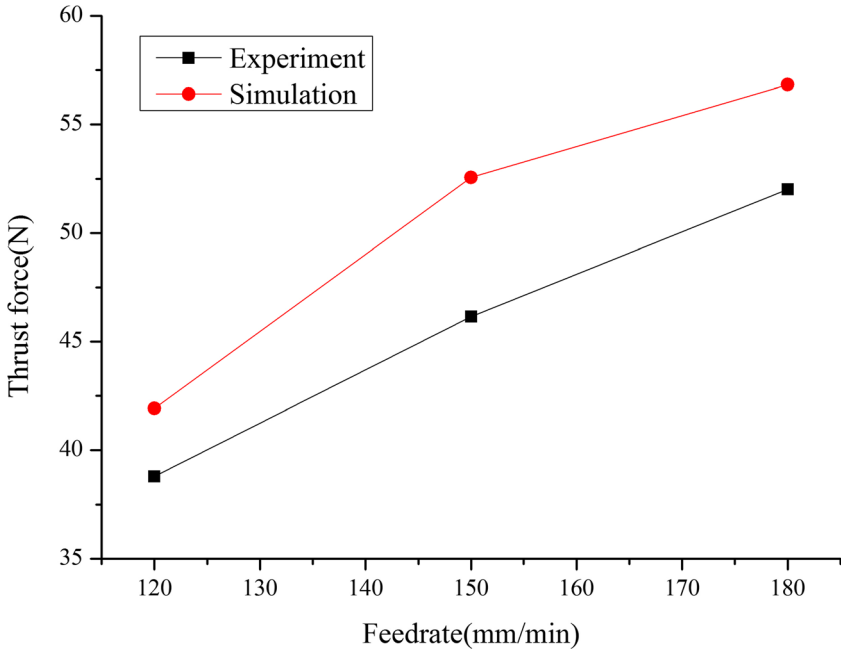

Fig. 8 Effects of feedrate on thrust force

5 Results and discussions

5.1 Analysis of thrust force

Model validation is carried out by comparing experimental and simulated thrust forces. Maximum thrust forces (being the peak value of the thrust force evolution versus cutting time) are obtained from the experimental measurement and the numerical simulations. Table 3 shows all the numerical values of experimental tests and FEA results. Figure 7 shows the thrust force evolution versus cutting time for the first case in Table 3.

For this first case in Table 3, the spindle speed is equal to 3000 rpm and the feedrate is equal to 120 mmpm. The average maximum thrust forces in the steady status (being in the green dash lines boxes shown in the Fig. 7) are 38.79 and 41.92 N, respectively. This shows that the FE model estimates the thrust force accurately with 8.07% deviation from the test results. A

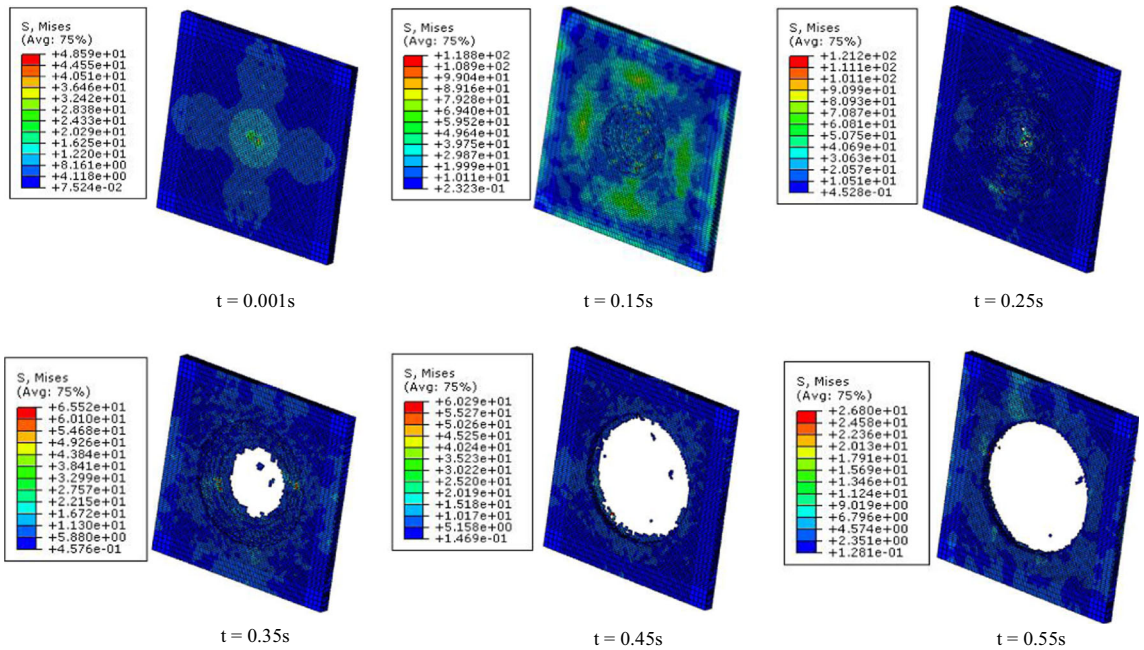

Fig. 9 Stress distributions in the drilling of 2.5D C/C composite plate (n = 3000 rpm, v_f = 120 mmpm)

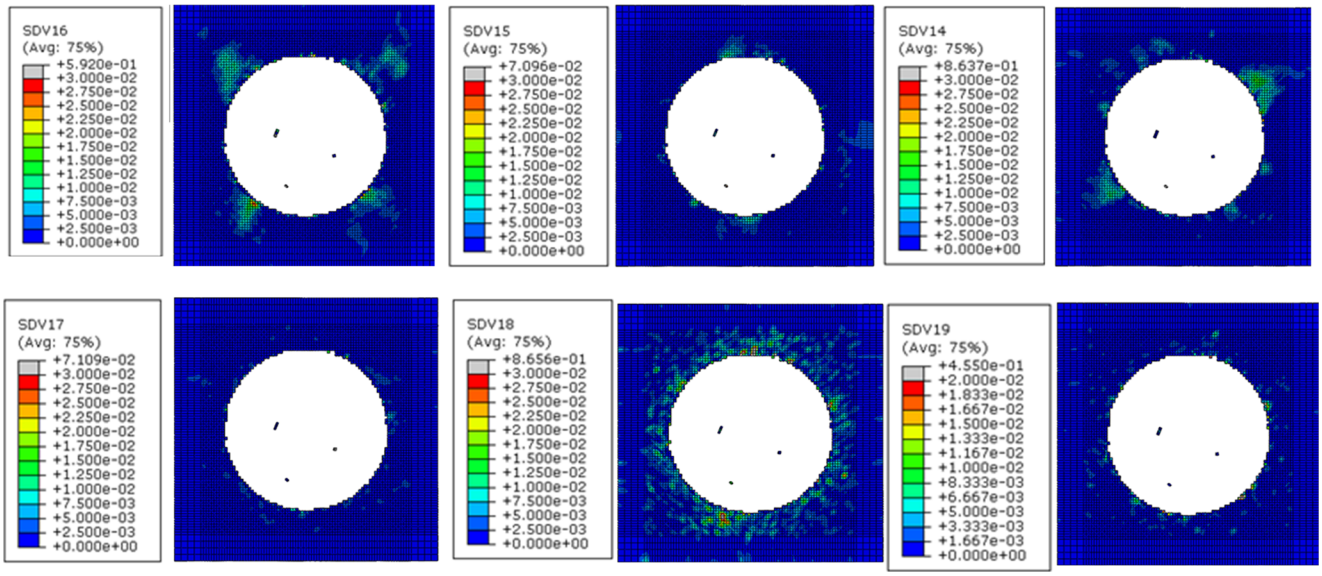

Fig. 10 Progressive damage analysis of workpiece (n = 3000 rpm, v_f = 180 mmpm)

good agreement between measured and predicted thrust forces can be found from Fig. 7. In the steady status, it can be seen from Fig. 7 that the experimental values of thrust force changed from 9.41 to 48.59 N, while the FE model estimated results changed from 8.27 to 50.55 N. In the second and third cases, the maximum relative differences are about 13.86 and 9.27%, respectively. This result agrees well with conclusion in literature [11], in which the maximum relative difference between the experimental value and the predicted value by regression equations is 13.8% for the thrust force. The result gives the confidence about the capability of the FE model in its prediction of the thrust forces for drilling of 2.5D C/C composites.

Figure 8 shows the effect of feedrate on the average maximum thrust force. The FE model estimates the thrust force between 41.92 and 56.83 N for the ranges of feedrates selected. The obtained results indicate that thrust force in drilling increases with the increasing feedrate. It can be seen from Fig. 8 that the average maximum thrust force is the highest at the feedrate of 180 mmpm and lowest at the feedrate of 120 mmpm for the constant spindle speed of 3000 rpm. Comparing the levels of experimental and FE simulation thrust forces for different feedrates, it can be observed that when feedrate is changed from 120 to 180 mmpm, the thrust force increases by 34 and 36%, respectively.

5.2 Analysis of stress in the workpiece

The progressive damage and the stress distributions of the 2.5D C/C composite plate during the drilling process are shown in Fig. 9. The total drilling time is 0.55 s. It can be observed from the images that stress is induced in the workpiece as the drill touches the workpiece material surface. The maximum stress is about 120 Mpa when t = 0.25 s. As the drill

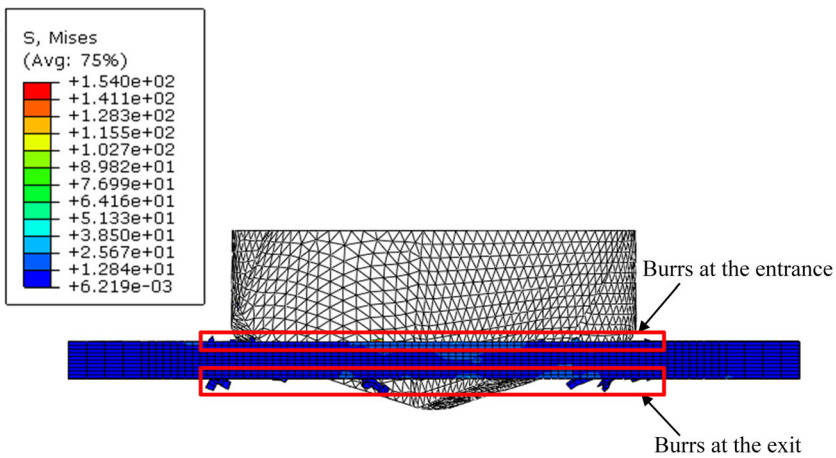

Fig. 11 Simulation results of burrs at the entrance and exit of the hole edges

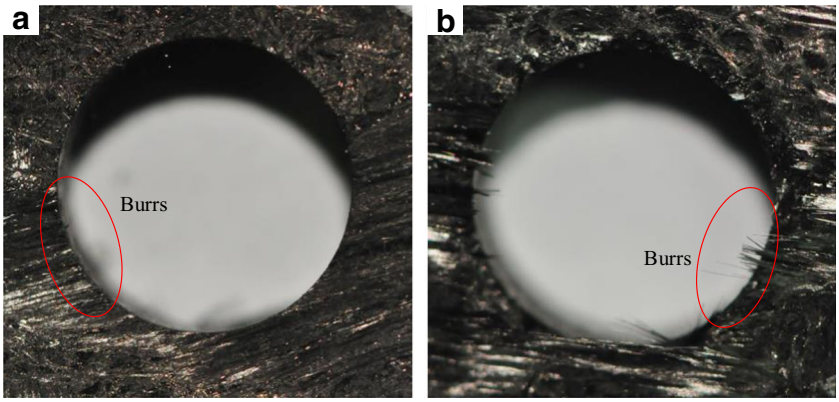

Fig. 12 Experimental results of burrs at the entrance and exit of the hole edges (n = 3000 rpm, v_f = 180 mmpm). **a** Entrance; **b** exit

moves into the material, the material continues to fail according to the damage model. When the elements fail completely, they are removed from the model. As the drilling process is finished (t = 0.55 s), the residual stress is about 16 Mpa.

5.3 Analysis of damage

Figure 10 shows the contour plots of progressive damage of the 2.5D C/C composite workpiece at the time of 0.37 s of drilling process in case of the spindle speed is 3000 rpm and the feedrate is 180 mmpm. The subfigures SDV14, SDV15, SDV16, SDV17, SDV18, and SDV19 represent the damage revolution of the X-direction fiber-matrix tension, X-direction fiber-matrix compression, Y-direction tension, Y-direction compression, normal tension, and normal compression. When the values of failure factors e_x^t, e_x^c, e_y^t, e_y^c, e_z^t, and e_z^c reach to 1, failure in that mode occurs.

It can be observed from the images that damages distribute around the hole edge randomly and decrease gradually along the radial direction. The maximum damage variables of X-direction fiber-matrix tension and compression are 0.86 and 0.07, respectively. The maximum damage variables of Y-direction tension and compression are 0.59 and 0.07, respectively. The maximum damage variables of normal tension and compression are 0.87 and 0.46, respectively. Damages are mainly caused by tensile stress, and tensile damages are more serious than compression damages. The most serious damage located in the normal direction since the tensile failure strength in the normal direction is lower comparing to compressive failure strength. Moreover, the tensile failure strength in the normal direction also is far lower than that in the X- and Y-directions.

Figure 11 shows the FE simulation results of burrs at the edge of entrance and exit in drilling of 2.5D C/C composite plate. Figure 12 shows the experimental results of burrs at the entrance and exit of the hole after drilling. It can be observed from these images that the burrs at the exit edge are more serious than the entrance. This corresponds with not only the experimental results, but also it agrees with the conclusions in [44]: Feedrate acts as the most important factor that influences damage at the entrance of the hole, and cutting speed serves as the key factor that affects the damage at the exit of the hole.

6 Conclusions

In this paper, the effect of cutting parameters on thrust force in drilling of a 2.5D C/C composite plate is investigated both experimentally and numerically. A 3D FEA method for drilling of 2.5D C/C composites is presented.

A user-defined 3D damage model (VUMAT) for the prediction of thrust force is developed and implemented in the FE code Abaqus/Explicit. An improved damage initiation model for drilling of 2.5D C/C composites is developed based on the Shokrieh-Lessard's model and the Hashin's failure criteria. Six different damage initiation mechanisms, namely X-direction fiber-matrix tension, X-direction fiber-matrix compression, Y-direction tension, Y-direction compression, normal tension, and normal compression, are considered and modeled separately. In order to approximate real failure process of 2.5D C/C composites, an improved 3D progressive failure model is modeled in detail.

The element–deletion approach based on the threshold stress levels in 2.5D C/C composites is implemented in the material model to allow for the hole-making process in drilling. The FE model predicts the drilling thrust force with 8.07 to 13.86% deviation when compared to experimental results, which is a reasonable accuracy. Moreover, the FE model can predict material failure process and damage with different cutting parameters in drilling of 2.5D C/C composites. The following conclusions are found from the verification experience:

- Cutting parameters have a significant influence on the stress, thrust force, and damage in drilling of 2.5D C/C composites. The thrust force and damage increase with the feedrate, but lower thrust force and damage can be get with the increase of cutting speed. Since burrs at the exit

edge are more serious than the entrance, cutting parameters should be adjusted accordingly at different period: at the exit of the hole, lower feedrate, and higher cutting speed can reduce damage.

- Tensile damages are more serious than compression damages in drilling of 2.5D C/C composites; this is owing to the fact that tensile stress is larger than compression stress. In addition, the most serious damage locates in the normal direction since the tensile failure strength in the normal direction is lower comparing to compressive failure strength. Moreover, the tensile failure strength in the normal direction also is far lower than that in the X- and Y-directions.

Generally, in order to achieve high accurate results for prediction of thrust force and damage in drilling of C/C composites, very fine mesh is essential. However, a more precise simulation has high requirement on computing resources. It can be seen that the accuracy of the predicted thrust force with different process parameters still needs to be improved, not only a more realistic friction model but also an enhanced damage model and thermal effects should be considered into the FE model, which consists of the future work of this study.

Acknowledgements This work is supported by "the National Natural Science Foundation of China (No. 51105312)" and "the Fundamental Research Funds for the Central Universities (NO.3102017gx06007)."

References

1. Christ K, Hüttinger K (1993) Carbon-fiber-reinforced carbon composites fabricated with mesophase pitch. Carbon 31(5):731–750
2. Savage G (1993) Applications of Carbon-carbon composites. Springer
3. Buckley JD (1988) Carbon-carbon-an overview
4. Windhorst T, Blount G (1997) Carbon-carbon composites: a summary of recent developments and applications. Mater Des 18(1): 11–15. doi:10.1016/S0261-3069(97)00024-1
5. Shan C, Wang X, Yang X, Lyu X (2016) Prediction of cutting forces in ball-end milling of 2.5D C/C composites. Chin J Aeronaut 29(3): 824–830. doi:10.1016/j.cja.2015.12.015
6. George PM, Raghunath BK, Manocha LM, Warrier AM (2004) EDM machining of carbon–carbon composite—a Taguchi approach. J Mater Process Technol 145(1):66–71. doi:10.1016/S0924-0136(03)00863-X
7. Hocheng H, Guu YH, Tai NH (1998) The feasibility analysis of electrical-discharge machining of carbon-carbon composites. Mater Manuf Process 13(1):117–132. doi:10.1080/10426919808935223
8. Kim D, Ramulu M (2004) Drilling process optimization for graphite/bismaleimide–titanium alloy stacks. Compos Struct 63(1):101–114. doi:10.1016/S0263-8223(03)00137-5
9. Singh I, Bhatnagar N (2006) Drilling-induced damage in unidirectional glass fiber reinforced plastic (UD-GFRP) composite laminates. Int J Adv Manuf Technol 27(9):877–882. doi:10.1007/s00170-004-2282-5
10. Ferreira J, Coppini N, Neto FL (2001) Characteristics of carbon–carbon composite turning. J Mater Process Technol 109(1):65–71
11. Li ZD, Zhao B, Tong JL, Duan P (2014) Study of carbon/carbon composite material surface morphology on ultrasonic vibration assisted milling. Key Eng Mater 579:181–185
12. Shan C, Lin X, Wang X, Yan J, Cui D (2015) Defect analysis in drilling needle-punched carbon–carbon composites perpendicular to nonwoven fabrics. Adv Mech Eng 7(8):1–11. doi:10.1177/1687814015598494
13. Krishnaraj V, Zitoune R, Davim JP (2013) Drilling of polymer-matrix composites. Springer, Heidelberg
14. Abrao A, Rubio JC, Faria P, Davim JP (2008) The effect of cutting tool geometry on thrust force and delamination when drilling glass fibre reinforced plastic composite. Mater Des 29(2):508–513
15. Rubio JC, Abrao A, Faria P, Correia AE, Davim JP (2008) Effects of high speed in the drilling of glass fibre reinforced plastic: evaluation of the delamination factor. Int J Mach Tools Manuf 48(6): 715–720
16. Davim JP, Rubio JC, Abrao A (2007) A novel approach based on digital image analysis to evaluate the delamination factor after drilling composite laminates. Compos Sci Technol 67(9):1939–1945
17. Gaitonde V, Karnik S, Rubio JC, Correia AE, Abrao A, Davim JP (2008) Analysis of parametric influence on delamination in high-speed drilling of carbon fiber reinforced plastic composites. J Mater Process Technol 203(1):431–438
18. Singh I, Bhatnagar N (2006) Drilling of uni-directional glass fiber reinforced plastic (UD-GFRP) composite laminates. Int J Adv Manuf Technol 27(9):870–876. doi:10.1007/s00170-004-2280-7
19. Feito N, Diaz-Álvarez J, López-Puente J, Miguelez MH (2016) Numerical analysis of the influence of tool wear and special cutting geometry when drilling woven CFRPs. Compos Struct 138:285–294. doi:10.1016/j.compstruct.2015.11.065
20. Davim JP (2009) Drilling of composite materials. NOVA Publishers, New York
21. Dandekar CR, Shin YC (2012) Modeling of machining of composite materials: a review. Int J Mach Tools Manuf 57:102–121. doi:10.1016/j.ijmachtools.2012.01.006
22. Liu D, Tang Y, Cong WL (2012) A review of mechanical drilling for composite laminates. Compos Struct 94(4):1265–1279. doi:10.1016/j.compstruct.2011.11.024
23. Bandhu D, Sangwan SS, Verma M (2014) A review of drilling of carbon fiber reinforced plastic composite materials. Int J Curr Eng Technol 14(3):1749–1752
24. Arola D, Ramulu M (1997) Orthogonal cutting of fiber-reinforced composites: a finite element analysis. Int J Mech Sci 39(5):597–613. doi:10.1016/S0020-7403(96)00061-6
25. Santiuste C, Soldani X, Miguélez MH (2010) Machining FEM model of long fiber composites for aeronautical components. Compos Struct 92(3):691–698. doi:10.1016/j.compstruct.2009.09.021
26. Soldani X, Santiuste C, Muñoz-Sánchez A, Miguélez MH (2011) Influence of tool geometry and numerical parameters when modeling orthogonal cutting of LFRP composites. Compos Part A 42(9): 1205–1216. doi:10.1016/j.compositesa.2011.04.023
27. Santiuste C, Olmedo A, Soldani X, Miguélez H (2012) Delamination prediction in orthogonal machining of carbon long fiber-reinforced polymer composites. J Reinf Plast Compos 31(13): 875–885
28. Zitoune R, Collombet F (2007) Numerical prediction of the thrust force responsible of delamination during the drilling of the long-fibre composite structures. Compos Part A 38(3):858–866. doi:10.1016/j.compositesa.2006.07.009
29. Durão LMP, de Moura MFSF, Marques AT (2008) Numerical prediction of delamination onset in carbon/epoxy composites drilling. Eng Fract Mech 75(9):2767–2778. doi:10.1016/j.engfracmech.2007.03.009
30. Isbilir O, Ghassemieh E (2012) Finite element analysis of Drilling of carbon fibre reinforced composites. Appl Compos Mater 19(3): 637–656. doi:10.1007/s10443-011-9224-9

31. Hashin Z (1981) Fatigue failure criteria for unidirectional fiber composites. J Appl Mech 48(4):846–852. doi:10.1115/1.3157744
32. Isbilir O, Ghassemieh E (2013) Numerical investigation of the effects of drill geometry on drilling induced delamination of carbon fiber reinforced composites. Compos Struct 105:126–133. doi:10.1016/j.compstruct.2013.04.026
33. Phadnis VA, Makhdum F, Roy A, Silberschmidt VV (2013) Drilling in carbon/epoxy composites: experimental investigations and finite element implementation. Compos Part A 47:41–51. doi:10.1016/j.compositesa.2012.11.020
34. Puck A, Schürmann H (1998) Failure analysis of FRP laminates by means of physically based phenomenologicaL Models1. Compos Sci Technol 58(7):1045–1067. doi:10.1016/S0266-3538(96)00140-6
35. Orifici AC, Herszberg I, Thomson RS (2008) Review of methodologies for composite material modelling incorporating failure. Compos Struct 86(1–3):194–210. doi:10.1016/j.compstruct.2008.03.007
36. Shokrieh MM, Lessard LB (2000) Progressive fatigue damage modeling of composite materials, part I: modeling. J Compos Mater 34(13):1056–1080. doi:10.1177/002199830003401301
37. Kachanov L (2013) Introduction to continuum damage mechanics, vol 10. Springer Science & Business Media
38. Falzon BG, Apruzzese P (2011) Numerical analysis of intralaminar failure mechanisms in composite structures. Part I: FE implementation. Compos Struct 93(2):1039–1046. doi:10.1016/j.compstruct.2010.06.028
39. Lapczyk I, Hurtado JA (2007) Progressive damage modeling in fiber-reinforced materials. Compos Part A 38(11):2333–2341. doi:10.1016/j.compositesa.2007.01.017
40. Qinlu Y, Yulong L, Hejun L, Shuping L, Lingjun G (2008) Quasi-static and dynamic compressive fracture behavior of carbon/carbon composites. Carbon 46(4):699–703. doi:10.1016/j.carbon.2008.01.031
41. Falzon BG, Apruzzese P (2011) Numerical analysis of intralaminar failure mechanisms in composite structures. Part II: applications. Compos Struct 93(2):1047–1053. doi:10.1016/j.compstruct.2010.06.022
42. Bažant ZP, Oh BH (1983) Crack band theory for fracture of concrete. Mater Constr 16(3):155–177. doi:10.1007/bf02486267
43. Klinkova O, Rech J, Drapier S, Bergheau J-M (2011) Characterization of friction properties at the workmaterial/cutting tool interface during the machining of randomly structured carbon fibers reinforced polymer with carbide tools under dry conditions. Tribol Int 44(12):2050–2058. doi:10.1016/j.triboint.2011.09.006
44. Davim JP (2009) Machining composite materials. NOVA Publishers, London